Influence of Ar_2^+ in an argon collisional-radiative model

Arnaud Bultel,* Bruno van Ootegem, Anne Bourdon, and Pierre Vervisch

*CORIA, UMR CNRS 6614, Université de Rouen, Site Universitaire du Madrillet, Avenue de l'Université,
76801 Saint-Etienne du Rouvray Cedex, France*

A nonlinear time-dependent collisional-radiative model for recombining argon is presented. Reactions involving Ar_2^+ are taken into account and their influence is discussed. It is shown that Ar_2^+ may increase the time to reach the quasi-steady-state by a factor of 100. The calculation of the recombination rate coefficient at the quasi-steady-state is presented. An analytical expression is derived and compared with existing literature values. The importance of the increase of the quasi-steady-state time is illustrated by comparisons of excited levels population densities distribution measured in a fast moving plasma where the mechanical time scale is sufficiently short to provide a time-dependent chemistry in a reference frame moving with the flow. The high sensitivity of the results towards the electron number density is pointed out. Finally, the influence of the processes involving Ar_2^+ on the excitation temperature is discussed.

I. INTRODUCTION

Collisional-radiative (CR) models are suitable tools to study chemical reactions in plasmas. Their main interest is indeed to access to the source term of the balance equation of a species. Applied to the case of an argon plasma for a particular excited level denoted $Ar(i)$, one can calculate the source term $\{\partial[Ar(i)]/\partial t\}_C$ of the balance equation (Litvak and Edwards [1]),

$$\frac{D[Ar(i)]}{Dt} + [Ar(i)]\vec{\nabla}\cdot\vec{v} = -\vec{\nabla}\cdot\vec{J_i} + \left(\frac{\partial[Ar(i)]}{\partial t}\right)_C, \quad (1)$$

where D/Dt is the hydrodynamic derivative, $\vec{v}$ the flow velocity, and $\vec{J_i}$ the flux density vector for $Ar(i)$.

Each term of the latter equation has a different characteristic time according to the physical situation. Generally for excited states, the time scale of $\{\partial[Ar(i)]/\partial t\}_C$ is largely shorter than the others: in this case, Eq. (1) indicates that $[Ar(i)]$ is governed only by chemical reactions. In addition, if the plasma is in stationary conditions for a velocity not too high $(D/Dt \simeq \partial/\partial t = 0)$, this density is in a quasi-steady-state. The CR model allows, therefore, the identification of the main processes responsible of the excited atom concentrations measured as well as the calculation of global rate coefficient: the rate coefficients of ionization, recombination, or dissociation are thus called collisional radiative. Numerous models (Sarrette *et al.* [2], Debal *et al.* [3], Kunc and Soon [4], Biberman *et al.* [5]) have been elaborated for various atoms and mixtures without calculating directly the time evolution of the species only due to the various chemical processes involved, that is, solving the balance equation neglecting the $\vec{\nabla}$ terms that prevent to verify that the time scale is really sufficiently short. For low-speed plasmas, the solution obtained by this way is valid for comparisons between

measured and calculated $[Ar(i)]$ when the electron density n_e is sufficiently high to ensure short time scales and sufficiently low to minimize diffusion (Drawin [6]). This is commonly observed in glow discharges and positive columns for the most excited states. The CR model appears hence to be a basic powerful element of plasma studies.

Particular situations lead to consider more terms in the balance equation. Indeed, for the metastable atoms for instance, the chemical time scale is longer than in the previous case and becomes of the same order of magnitude as the diffusion one: the comparison with experimental data has to be done considering the influence of $-\vec{\nabla}\cdot\vec{J_i}$ in the balance equation (Bogaerts and Gijbels [7]). In the case of fast moving plasmas as highly expanded jets, the situation is more complicated: the characteristic time associated to the convective derivative D/Dt may decrease sufficiently to give a significant role to the hydrodynamics even for highly excited atoms. Although the plasma is steady, that is, $\partial[Ar(i)]/\partial t = 0$, the chemical reactions source term $\{\partial[Ar(i)]/\partial t\}_C$ may be time dependent. Therefore, the calculation of the temporal evolution of the population densities only due to chemistry is needed.

On the other hand, Bogaerts and Gijbels [8] have recently pointed out the important role of Ar_2^+ on the kinetics of a direct current argon glow discharge in low pressure and electron density conditions. The relative contribution to the loss of electrons by dissociative recombination remains to be the most important one after the diffusion to the walls in their conditions. In the case of plasmas with $p > 500$ Pa, the level of pressure is sufficiently high to provide additional reactions involving Ar_2^+ that may lead to a strong variation of the electron density.

In the present paper, we propose to focus our attention on these two important points: (1) the time dependent chemistry of a weakly ionized argon plasma and (2) its dependence on the Ar_2^+ reactions. This study is based on the elaboration of a time dependent collisional-radiative model over the ranges $3000 \leq T_e \leq 12\,000$ K for the electron temperature and $10^{16} \leq n_e \leq 10^{21}$ m^{-3} for the electron density. After the presenta-

*Electronic address: Arnaud.Bultel@coria.fr
URL: http://www.coria.fr/

tion of the energetic diagram adopted, we describe all elementary processes taken into account: the radiative processes, the electron induced processes for which the cross sections have been updated, those due to inelastic atom collisions for which a new model is proposed, and finally those involving the molecular ion Ar_2^+.

Two experimental works of reference are considered for comparison and discussion. First, Marie [9] has measured over a wide range of energy by various methods the population density of numerous excited levels in a highly ionized argon plasma: the good agreement with the results of the CR model in these conditions is a verification of the global consistency of the model. Second, van Ootegem [10] has experimentally studied a highly expanded and weakly ionized plasma at relatively high pressure in order to investigate the electron density fluctuations in the trailing wake of ballistic missiles. We demonstrate that the order of magnitude of the parameters measured can be understood in the light of the Ar_2^+ influence and time scale considerations.

II. ATOMIC MODEL

We consider three types of particles in this CR model: atoms (in fundamental and excited levels), Ar^+ and Ar_2^+ ions, and electrons. Molecular argon Ar_2 is not considered. First, the dissociation limit of its ground-state level ($X\,^1\Sigma_g^+$) is approximately 0.01 eV (Freeman and Yoshino [11]), which is considerably less than the order of magnitude of the thermal energy considered in this paper. Moreover, the rate coefficient of formation of excited molecules in these thermal conditions are largely less than those for the formation of Ar_2^+ (Lam *et al.* [12], Brunet *et al.* [13]). In addition, the examination of the potential energy curves of Ar_2 reveals for the lowest states few nondissociative levels (Yates and Ermler [14], Castex *et al.* [15]), which may play a significant role in the kinetics.

The Ar atom follows essentially the (j,l) coupling: the core electrons are independent of the state of the outer electron responsible for the excitation of the atom. This electron is characterized by the principal quantum number n and the values of the orbital quantum number l and spin quantum number s. The atomic core has the {Mg}-$3p^5$ structure, its angular momentum depends on the configuration of the last $3p$ electron, all the others being compensated. Since $l=1$ and $s=1/2$ for this electron, the core angular momentum may have two possible values: $j_c=l+s=3/2$ and $j_c=l-s=1/2$. This particularity yields to two ionization limits with slightly different energies. The first core configuration ($j_c=3/2$), also called "nonprimed" subsystem, has an ionization limit $E_{ion}=15.760$ eV and the second one ($j_c=1/2$), called the "primed" subsystem, $E_{ion}=15.937$ eV.

Due to this quantum effect, the 64 excited levels considered here are separated into two groups according to the value of j_c. The energetic diagram follows the Vlček's one [16] (cf. Table I) recently used by Bogaerts *et al.* [17]. It contains real levels as the metastable ones and fictitious levels corresponding to groups of close energy (Katsonis and Drawin [18]). There are 32 levels of energy greater than

15.45 eV. The subsystems of core configuration give rise to two types of Ar^+ of statistical weights equal to 4 for the "nonprimed" one and 2 for the other one.

Finally, we consider Ar_2^+ ions that have an important influence on the kinetics as will be pointed out in the following. The fundamental level being of the $^2\Sigma_u^+$ type (Wadt [19]), its statistical weight is 2.

III. COLLISIONAL AND RADIATIVE PROCESSES

A. Spontaneous emission

We have used Natl. Bur. Stand. (U.S.) tables [20] and more recent results of Wiese *et al.* [21] as basic data. Verner *et al.* [22] have done a compilation concerning resonance lines. Among them, we found data about transitions in argon between some excited levels with energy higher than 14 eV and the ground state. In our conditions, the population density of the ground state is high enough to have a complete self-absorption, therefore, we have assumed no emission.

The self-absorption is taken into account for other transitions under the form of the calculation of the classical radiative Holstein escape factors [16]. Moreover, since the energetic diagram contains fictitious levels, each effective transition probability has been calculated from individual ones by weighting with the degeneracy factors.

The table of all transition probabilities will be available on the website of our laboratory.

B. Radiative recombination

Concerning the radiative recombination, that is,

$$Ar^+(j_c)+e^-\rightarrow Ar(i)+h\nu,$$
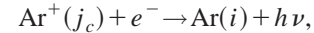
we have just taken into account transitions straightforward to the $3p^54s$ levels (between 11.5 eV and 12 eV). We assumed that the process to the ground state is negligible due to the complete self-absorption resulting because of the high order of magnitude of its population density. Moreover, for transitions to levels of energy higher than 12.9 eV ($3p^54p$), the process is neglected since the radiative recombination cross section depends on n_i^{*-3} where n_i^* is the effective quantum number.

The cross section adopted for this process is the following:

$$\sigma_{ion-i}^R(\epsilon)=\frac{g_i}{2\,g_{ion}(j_c)}\frac{(h\nu)^2}{m_ec^2}\frac{1}{\epsilon}\sigma_{i\text{-}ion}^P(h\nu),\qquad(2)$$

where g_i and $g_{ion}(j_c)$ are, respectively, the statistical weight of the i level and of $Ar^+(j_c)$, m_e the electron mass, c the speed of light, and $\sigma_{i\text{-}ion}^P$ the photoionization cross section. $h\nu=\epsilon+E_{ion}-E(i)$ is the energy of the photon produced. The value of j_c is the same for the excited $Ar(i)$ atom.

TABLE I. List of energy levels used in this CR model.

n_g	$E(n_g)$	g_{n_g}	j_c	$n\,l\,[K]_J$	n_g	$E(n_g)$	g_{n_g}	j_c	$n\,l\,[K]_J$
1	0	1	1.5	$3p^6$	34	15.460	48	1.5	$7d,\,9s$
2	11.548	5	1.5	$4s[3/2]_2$	35	15.461	12	0.5	$7p$
3	11.624	3	1.5	$4s[3/2]_1$	36	15.482	320	1.5	$7f,\,7g,\,7h,\,7i$
4	11.723	1	0.5	$4s[1/2]_0$	37	15.520	24	0.5	$6d,\,8s$
5	11.828	3	0.5	$4s[1/2]_1$	38	15.548	480	1.5	$8d,\,8f,\,\ldots,$
6	12.907	3	1.5	$4p[1/2]_1$	39	15.560	108	0.5	$6f,\,6g,\,6h$
7	13.116	20	1.5	$4p[3/2]_{1,2},\,4p[5/2]_{2,3}$	40	15.592	640	1.5	$9p,\,9d,\,9f,\,\ldots,$
8	13.273	1	1.5	$4p[1/2]_0$	41	15.600	12	0.5	$8p$
9	13.295	8	0.5	$4p[3/2]_{1,2}$	42	15.624	800	1.5	$10s,\,\ldots,$
10	13.328	3	0.5	$4p[1/2]_1$	43	15.636	24	0.5	$7d,\,9s$
11	13.480	1	0.5	$4p[1/2]_0$	44	15.648	968	1.5	$11s,\,\ldots,$
12	13.884	9	1.5	$3d[1/2]_{0,1},\,3d[3/2]_2$	45	15.659	160	0.5	$7f,\,7g,\,7h,\,\ldots,$
13	13.994	16	1.5	$3d[7/2]_{3,4}$	46	15.666	1152	1.5	$12s,\,\ldots,$
14	14.090	23	1.5	$3d[3/2]_1,\,3d[5/2]_{2,3},\,5s$	47	15.680	1352	1.5	$13s,\,\ldots,$
15	14.229	17	0.5	$3d[3/2]_2,\,3d[5/2]_{2,3}$	48	15.691	1568	1.5	$14s,\,\ldots,$
16	14.252	4	0.5	$5s$	49	15.700	1800	1.5	$15s,\,\ldots,$
17	14.304	3	0.5	$3d[3/2]_1$	50	15.707	2048	1.5	$16s,\,\ldots,$
18	14.509	24	1.5	$5p$	51	15.713	2312	1.5	$17s,\,\ldots,$
19	14.690	12	0.5	$5p$	52	15.718	2592	1.5	$18s,\,\ldots,$
20	14.792	48	1.5	$4d,\,6s$	53	15.722	2888	1.5	$19s,\,\ldots,$
21	14.906	56	1.5	$4f$	54	15.725	240	0.5	$8d,\,8f,\,\ldots,$
22	14.976	24	0.5	$4d,\,6s$	55	15.769	320	0.5	$9p,\,9d,\,9f,\,\ldots,$
23	15.028	24	1.5	$6p$	56	15.801	400	0.5	$10s,\,\ldots,$
24	15.083	28	0.5	$4f$	57	15.825	484	0.5	$11s,\,\ldots,$
25	15.153	48	1.5	$5d,\,7s$	58	15.843	576	0.5	$12s,\,\ldots,$
26	15.205	12	0.5	$6p$	59	15.857	676	0.5	$13s,\,\ldots,$
27	15.215	128	1.5	$5f,\,5g$	60	15.868	784	0.5	$14s,\,\ldots,$
28	15.282	24	1.5	$7p$	61	15.877	900	0.5	$15s,\,\ldots,$
29	15.324	24	0.5	$5d,\,7s$	62	15.884	1024	0.5	$16s,\,\ldots,$
30	15.347	48	1.5	$6d,\,8s$	63	15.890	1156	0.5	$17s,\,\ldots,$
31	15.382	216	1.5	$6f,\,6g,\,6h$	64	15.895	1296	0.5	$18s,\,\ldots,$
32	15.393	64	0.5	$6d,\,8s$	65	15.899	1444	0.5	$19s,\,\ldots,$
33	15.423	24	1.5	$8p$					

Finally, the photoionization cross section expressed in m^2 is [16]

$$\sigma_{i\text{-ion}}^{P}(h\nu)=2\times10^{-22}\lambda_i \quad \text{for } E_{\text{ion}}-E(i)\leq h\nu\leq 0.59\,E_{\text{ion}}^{H},$$

$$(3a)$$

$$\sigma_{i\text{-ion}}^{P}(h\nu)=7.91\times10^{-22}\lambda_i\left(\frac{E_{\text{ion}}-E(i)}{E_{\text{ion}}^{H}}\right)^{2.5}$$

$$\times\left(\frac{E_{\text{ion}}^{H}}{h\nu}\right)^{3}\quad\text{for } h\nu>0.59\,E_{\text{ion}}^{H},\qquad(3b)$$

with $\lambda_i=0.0763$ for $i=2$, 0.0458 for $i=3$, 0.0305 for $i=4$, and 0.0915 for $i=5$.

C. Electron induced processes

In a general manner, the static and dynamic screening effects have been neglected. Indeed, the level of electron density ($10^{16}\leq n_e\leq10^{21}$ m^{-3}) as well as electron temperature ($3000\leq T_e\leq12\,000$ K) are too weak to introduce important discrepancies in relation to the ideal case as pointed out by Bornath *et al.* [23] for hydrogen. As a result, the pressure ionization has not been considered (Salzmann [24]).

Few experimental data are available concerning the excitation by electron impact. It is well known that the analytical forms proposed by Drawin are particularly well adapted. Indeed, calculating their dependent parameters from the experimental results of the cross sections is sufficient. These expressions are the following.

For the optically allowed transitions ($\Delta l=\pm1$, $\Delta J=0$, ±1 except $J=0\rightarrow J=0$),

$$\sigma_{ij}^{e}(U_{ji})=4\pi a_0^2\left(\frac{E_{\text{ion}}^{H}}{E_{ji}}\right)^2\alpha_{ij}f_{ij}\frac{U_{ji}-1}{U_{ji}^2}\ln\left(\frac{5}{4}\beta_{ij}U_{ji}\right).\quad(4)$$

TABLE II. Parameters for the calculation of σ_{ij}^e. A, S, and P represent allowed, spin, and parity forbidden transitions, respectively, followed by the related references. j_c is related to intercombination transitions assumed impossible. When Ar^+ is mentioned, one gives the values $\alpha_{i\text{-ion}}$ and $\beta_{i\text{-ion}}$ for the ionization process.

i	j	Transition	Parameter	i	j	Transition	Parameter
1	2	S	0.111 [29–33]	2	8	S	0.98 [34–37]
1	3	A	0.0357, 4.0 [30–33]	2	9	A	0.075, 0.5 [34–37]
1	4	S	0.0177 [29–33]	2	10	A	0.019, 0.5 [34,36,37]
1	5	A	0.0813, 4.0 [31–33,38]	2	11	S	0.43 [34,37]
1	6	P	0.174 [33,38]	2	12,...,17	P	0.05 [25]
1	7	P	0.493 [33]	2	18	A	1.56×10^{-4}, 1.0 [39]
1	8	P	0.0322 [33]	2	19	j_c	0
1	9	P	0.107 [33]	3	4	P	0.05 [25]
1	10	P	0.0322 [33]	3	5	P	0.05 [25]
1	11	P	0.0105 [38]	3	6,...,11	A	0.019, 0.5 [40]
1	12	S	0.15 [41]	3	12,...,17	P	0.05 [25]
1	13	S	0.08 [41]	3	18	A	9.4×10^{-5}, 1.0 [39]
1	14	A	0.0333, 4.0 [41]	3	19	j_c	0
1	15	P	0.035 [41]	4	5	P	35 [34]
1	16	A	3.71×10^{-3}, 4.0 [41]	4	6	A	0.025, 4.0 [34]
1	17	A	0.0179, 4.0 [16]	4	7	A	0.043, 4.0 [34]
1	18	P	0.07 [16]	4	8	S	1.2 [34,37]
1	19	P	0.05 [16]	4	9	A	0.3, 0.5 [34–37]
1	20	A	0.0515, 1.0 [16]	4	10	A	0.19, 0.5 [34,36,37]
1	21	P	0.028 [41]	4	11	S	1.3 [34,37]
1	22	A	0.0306, 1.0 [16]	4	12,...,17	P	0.05 [25]
1	23	P	0.001 [16]	4	18	j_c	0
1	24	P	3.5×10^{-3} [41]	4	19	A	3.2×10^{-5}, 1.0 [39]
1	25	A	0.0369, 1.0 [16]	5	6,...,11	A	2.5×10^{-2}, 4.0 [42]
1	26,...,28	P	0.001 [16]	5	12,...,17	P	0.05 [25]
1	29	A	6.5×10^{-4}, 1.0 [16]	5	18	j_c	0
1	30	A	0.0024, 1.0 [16]	5	19	A	9.6×10^{-5}, 1.0 [39]
2	3	P	60 [34,35]	2,...,5	Ar^+	A	0.35, 4.0 [16]
2	4	P	7 [34]	6	Ar^+	A	0.45, 4.0 [16]
2	5	P	7 [34]	7,...,9	Ar^+	A	0.39, 4.0 [16]
2	6	A	0.05, 4.0 [34]	10,...,11	Ar^+	A	0.32, 4.0 [16]
2	7	A	0.38, 1.0 [34–37]	≥ 12	Ar^+	A	0.67, 1.0 [16]

For the parity forbidden transitions ($\Delta l \neq \pm 1$),

$$\sigma_{ij}^e(U_{ji}) = 4\pi a_0^2 \alpha_{ij}^P \frac{U_{ji}-1}{U_{ji}^2}.$$

For the spin forbidden transitions ($\Delta J \neq 0, \pm 1$ including $J = 0 \rightarrow J = 0$),

$$\sigma_{ij}^e(U_{ji}) = 4\pi a_0^2 \alpha_{ij}^S \frac{U_{ji}^2-1}{U_{ji}^5},$$

$U_{ji} = \epsilon/E_{ji}$ is the reduced kinetic energy ϵ of electron where $E_{ji} = E(j) - E(i)$, a_0 the first Bohr radius, E_{ion}^H the ionization energy of hydrogen atom in ground state, and f_{ij} the absorption oscillator strength.

The parameters $\alpha_{ij} f_{ij}$, β_{ij}, α_{ij}^P, and α_{ij}^S adopted are chosen in accordance with the more recent experimental investigations (see Table II). The results for low electron kinetic

energy are preferred due to the order of magnitude of the electron temperature. When several works may lead to different parameters, we have chosen the one allowing the best agreement with theoretical results. Finally, 75% of the apparent cross section measured have been considered for calculating the parameters in the case no other reference exists.

The transitions $2 \rightarrow 19$, $3 \rightarrow 19$, $4 \rightarrow 18$, and $5 \rightarrow 18$ have been removed since the intercombination reactions ($\Delta j_c \neq 0$) do not correspond to optically allowed, parity, or spin forbidden transitions.

About the other transitions for which no data are available, usual selection rules are used. The processes are assumed to be of the parity type when they are forbidden: it is the case for levels with i higher than 18 when $\Delta l \neq \pm 1$ since their quantum number J is not considered. The value adopted for α_{ij}^P is 5.0×10^{-2} as the average of the results of Kimura et al. [25]. When the transitions are optically allowed, the Drawin's equation is used with $\alpha_{ij} f_{ij} = 1.0$ and $\beta_{ij} = 1.0$ as-

suming possible the intercombination reactions only for j $\leqslant 41$. Beyond this limit, the excited electron is so far from the core that the likelihood for an inner change is almost zero.

Concerning the allowed transitions, we have tested also the expressions proposed by Vriens and Smeets [26] and Seaton [27]. We refer to their paper for more details. The population densities can also change due to the ionization by electron impact,

$$\mathrm{Ar}(i) + e^- \rightarrow \mathrm{Ar}^+(j_c) + 2\,e^-. \tag{5}$$
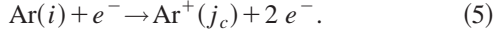
For the ground state, Straub *et al.* [28] have measured the ionization cross section that may be fitted by

$$\sigma_{1\text{-ion}}^e(\epsilon) = 2.79 \times 10^{-20} \ln\left(\frac{\epsilon}{15.760}\right) \ \mathrm{m}^2,$$

where ϵ is expressed in eV and such that $15.760 \leqslant \epsilon$ $\leqslant 40$ eV. Since the electron temperature T_e is less than 10^4 K, it is unnecessary to consider higher energies. For $2 \leqslant i \leqslant 11$, Drawin has proposed [16]

$$\sigma_{i\text{-ion}}^e(U_{\text{ion-}i}) = 4\pi a_0^2 \left(\frac{E_{\text{ion}}^H}{E_{\text{ion-}i}}\right)^2 \alpha_{i\text{-ion}}$$

$$\times \frac{U_{\text{ion-}i} - 1}{U_{\text{ion-}i}^2} \ln\left(\frac{5}{4}\beta_{i\text{-ion}} U_{\text{ion-}i}\right),$$

with $E_{\text{ion-}i} = E_{\text{ion}} - E_i$ and $U_{\text{ion-}i} = \epsilon/E_{\text{ion-}i}$.

Considering only no intercombination transitions, the value of j_c is a parameter for $U_{\text{ion-}i}$. The ionization occurs whatever may be the nature of the state considered, this restriction provides only a slight difference for the related rate coefficient with respect to the case in which the ionization limit should be equal to 15.76 eV. However, this influences further the recombination rate coefficient because [Ar$^+$] behave independently. As Vlcèk, the values $\alpha_{i\text{-ion}} = 0.67$ and $\beta_{i\text{-ion}} = 1$ are used for $i \geqslant 12$. Table II contains all required parameters.

D. Inelastic atom-atom collisions

As a result of the possible weakness of the ionization degree of the plasma, the reactions

$$\mathrm{Ar}(i) + \mathrm{Ar}(1) \rightarrow \mathrm{Ar}(j>i) + \mathrm{Ar}(1) \tag{6}$$
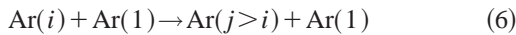
may play an important role and have been considered. Conversely, the antiscreening channel allowing the ionization of one of the colliders and the excitation or the ionization of the other one has been neglected since the thermal energy available is not sufficient and the cross sections are less than for the mechanism (6) by several orders of magnitude [43].

Haugsjaa and Amme [44] have determined the apparent excitation cross section of the $3p^54s$ levels from the ground state. The transitions $1 \rightarrow 2$ and $1 \rightarrow 4$ being optically forbidden, we have allocated this cross section to the optically allowed processes $1 \rightarrow 3$ and $1 \rightarrow 5$. The estimation of each contribution was done as follows. For the excitation by elec-

TABLE III. Parameters related to the atom-atom processes. The excitation from the ground state $i=1$ follows the equation $\sigma_{ij}^A = \beta_{ij}^*(\epsilon - E_{ji})$, for the others the equation $\sigma_{ij}^A = \beta_{ij}^*(\epsilon - E_{ji})/E_{ji}^{2.26}$ is used.

i	j	β_{ij}^*
1	3	2.10×10^{-25}
1	5	4.80×10^{-25}
2	3	1.79×10^{-24}
2	4	4.80×10^{-26}
2	5	4.80×10^{-26}
3	4	4.80×10^{-26}
3	5	4.80×10^{-26}
4	5	1.79×10^{-24}

tron impact, the cross section is much higher for the transition $1 \rightarrow 5$ than for $1 \rightarrow 3$ due to the quantum configuration of the levels involved. We have assumed a same ratio for the cross sections related to atom impact. The results of Haugsjaa and Amme allow to allocate for low energy a linear function to the cross section denoted σ_{1j}^A,

$$\sigma_{1j}^A(\epsilon) = \beta_{1j}^*(\epsilon - E_{j1}), \tag{7}$$

where ϵ is the relative kinetic energy of the colliding atoms and E_{j1} the energy difference. The collisions with low energy are of interest since the kinetic temperature, denoted T_A in the following, is relatively weak. Using Eq. (7), the parameter β_{1j}^* has been calculated (see Table III).

For inner $3p^54s$ manifold transitions, Bogaerts *et al.* [17] have expressed analytically the cross sections as

$$\sigma_{ij}^A(\epsilon) = \beta_{ij}^* \frac{\epsilon - E_{ji}}{E_{ji}^{2.26}}.$$

Table III contains the related values of the parameter β_{ij}^*. Whatever the other transitions between excited levels, we have assumed that no intercombination reactions occur.

For $i=1$, Haugsjaa and Amme [44] have also measured the ionization cross section,

$$\sigma_{1\text{-ion}}^A(\epsilon) = 1.8 \times 10^{-25}(\epsilon - 15.760)^{1.3} \ \mathrm{m}^2, \tag{8}$$

where the relative energy of colliding atoms ϵ is expressed in eV. We have used the cross section (8) finding no more accurate data in the literature.

Starting from the cross section deduced by Thomson [45] for electron induced ionization, Drawin [46] gave the following form for the cross section of ionization by atom impact:

$$\sigma_{i\text{-ion}}^A(\epsilon) = 4\pi a_0^2 \left(\frac{E_{\text{ion}}^H}{E_{\text{ion-}i}}\right)^2 \frac{m_A}{m_H} \xi_i^2 \frac{2\ \mathrm{m}_e}{m_A + m_e}$$

$$\times \frac{U_{\text{ion-}i}(\epsilon) - 1}{\{1 + [2\ \mathrm{m}_e/(m_A + m_e)][U_{\text{ion-}i}(\epsilon) - 1]\}^2}, \tag{9}$$

where m_e and m_A are the electron and atom masses respectively and $U_{\text{ion-}i}(\epsilon)$ the nondimensional group $\epsilon/E_{\text{ion-}i}$. ξ_i is the number of optical electrons that is equal to 6 for the ground state and 1 for the others. In the case $i \neq 1$, the previous expression has been used systematically.

The lack of experimental data about the excitation by atom impact is especially critical for the highly excited levels. The order of magnitude for the difference of energy between two adjacent levels being all the smallest that they are close to their ionization limit, the atom impact processes may play an important role for them although the temperature for heavy particles is small.

1. Drawin's model

Concerning the excitation between radiative coupled levels characterized by the absorption oscillator strength f_{ij}, Drawin [47,48] has adapted Eq. (9) under the form

$$\sigma_{ij}^A(\epsilon) = 4\pi a_0^2 \left(\frac{E_{\text{ion}}^H}{E_{ji}}\right)^2 \frac{m_A}{m_H} \xi_i^2 f_{ij} \frac{2m_e}{m_A + m_e}$$

$$\times \frac{U_{ji}(\epsilon) - 1}{\{1 + [2m_e/(m_A + m_e)][U_{ji}(\epsilon) - 1]\}^2}. \quad (10)$$

No form is proposed by Drawin for the forbidden transitions. That is the reason why Vlček [16] has plotted for the optically allowed transitions the values of $\sigma_{ij}^A/(\epsilon - E_{ji})$ as a function of E_{ji} with the help of rare experimental data and Eq. (10). Assuming the cross section to be a linear function of the relative energy ϵ near the threshold E_{ji} in the same way than Eq. (7), he obtained the following form for β_{ij}^* used when considering the Drawin's model:

$$\beta_{ij}^* = 8.69 \times 10^{-22} E_{ji}^{-2.26} \ \text{m}^2 \ \text{eV}^{-1}, \quad (11)$$

with E_{ji} expressed in eV.

2. Adapted model of Kaulakys

Among the highest 35 levels of the atomic model, most of them have a principal quantum number higher than 8. This situation corresponds to electronic shell where the peripheral electron is weakly linked to the nucleus [49]. For these levels, the conditions of Eq. (10) are not checked: using Eq. (11) may be questionable.

Our treatment of the inelastic collisions is based on the hypothesis that the peripheral electron (also called Rydberg electron) is almost free. The collision can Therefore, be understood as the elastic scattering of the electron on the incident atom. Its orbit changes so its momentum: the excitation of the target is modified.

Kaulakys [50] has developed a model for collisional angular momentum mixing of high Rydberg atoms, i.e.,

$$A(i,l) + B \rightarrow A(j) + B,$$

where B is an atom assumed without internal structure and l the orbital quantum number of the atom A having the principal quantum number i before collision and j after collision. He obtained the following equation:

$$\sigma_{i,l \rightarrow j}^A(g) = \pi \left(\frac{v_0}{g}\right)^2 \frac{1}{j^3} \int_{p_{\min}}^{+\infty} p^2 |\psi_{il}(p)|^2$$

$$\times \int_{\theta_{\min}}^{\pi} \cos\frac{\theta}{2} |f_{eB}(p,\theta)|^2 d\theta \, dp,$$

where $v_0 = \sqrt{2 E_{\text{ion}}^H/m_e}$ is a characteristic velocity for electron, $p_{\min} = |E_{j,il}|/2g$ the minimum value of the Rydberg electron momentum due to the excitation of the atom A, $\psi_{il}(p)$ the radial wave function of the electron in the state (i,l), $\theta_{\min} = 2\arcsin(p_{\min}/p)$ the minimum scattering angle and $f_{eB}(p,\theta)$ the differential elastic scattering amplitude between the electron and the atom B.

For our energetic diagram, we have to determine the total $i \rightarrow j$ cross section,

$$\sigma_{ij}^A(g) = \frac{1}{g_i} \sum_{l=0}^{i-1} (2l+1)\sigma_{i,l \rightarrow j}^A(g),$$

where g_i is the degeneracy factor of the level i. Since the principal quantum numbers are high, the energy of this level is almost independent of l. Moreover, $g_i = i^2$ and

$$\sum_{l=0}^{i-1} (2l+1)|\psi_{il}(p)|^2 = i^2 |\psi_i(p)|^2,$$

where $\psi_i(p)$ is the radial wave function of the Rydberg electron in the i state, with (Kaulakys [51])

$$|\psi_i(p)|^2 = \frac{32}{\pi} \frac{i^3}{[1 + i^2(p/m_e v_0)^2]^4}.$$

The cross section becomes

$$\sigma_{ij}^A(g) = \pi \left(\frac{v_0}{g}\right)^2 \frac{1}{j^3} \int_{p_{\min}}^{+\infty} p^2 |\psi_i(p)|^2$$

$$\times \int_{\theta_{\min}}^{\pi} \cos\frac{\theta}{2} |f_{eB}(p,\theta)|^2 d\theta \, dp.$$

Writing $k = p/m_e v_0$ the nondimensional momentum of the electron and $f_{eB}^*(k,\theta) = f_{eB}(p,\theta)/a_0$ the nondimensional differential elastic scattering amplitude, the cross section is finally

$$\sigma_{ij}^A(k_{\min}) = 16\pi a_0^2 \left(\frac{E_{\text{ion}}^H}{E_{ji}}\right)^2 \frac{1}{j^3} \gamma_i(k_{\min}),$$

where the i-level function $\gamma_i(k_{\min})$ is

$$\gamma_i(k_{\min}) = k_{\min}^2 \int_{k_{\min}}^{+\infty} k^2 |\psi_i(k)|^2$$

$$\times \int_{\theta_{\min}}^{+\infty} \cos\frac{\theta}{2} |f_{eB}^*(k,\theta)|^2 d\theta \, dk. \quad (12)$$
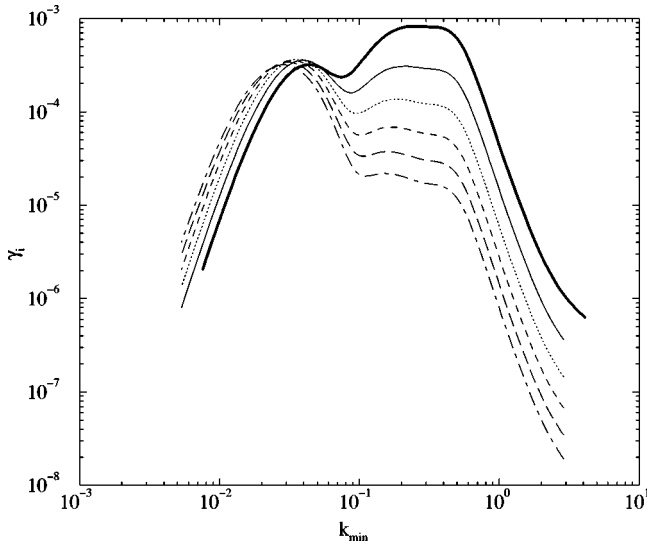
FIG. 1. Evolution of γ_i versus k_{min} for the calculation of the inelastic cross sections for atomic collisions derived from the work of Kaulakys. $i=8$, thick curve; $i=10$, solid curve; $i=12$, dotted curve; $i=14$, dashed curve; $i=16$, long-dashed curve; $i=18$, dot-dashed curve.

Weyhreter *et al.* [52] have experimentally determined the differential cross section of $e-$Ar elastic scattering on the energy range $0.05 \leqslant \epsilon \leqslant 2$ eV. This range corresponds to Ramsauer effect. We have used these results to calculate the function $\gamma_i(k_{min})$ by Eq. (12). Figure 1 illustrates the various functions deduced. We can observe the influence of the Ramsauer effect: in the vicinity of $k_{min} \simeq 10^{-1}$, γ_i decreases. In a general manner, the cross sections from the adapted model of Kaulakys are largely less than those from Vlček according to a factor sometimes equal to 100. The lower limit of the application of the model of Kaulakys is $i=8$ for considering Rydberg atoms (Lebedev and Fabrikant [53]). As a result, we have considered the Kaulakys model well adapted to the energy range 15.4 eV$<E_i<E_{ion}$. For the intermediate energies ($11.5<E_i<15.4$ eV), the model of Drawin has been applied.

E. Ar$_2^+$ processes

Ar$_2^+$ can be produced by Ar atomic to molecular ion conversion,

$$\text{Ar}^+(j_c=3/2)+\text{Ar}(1)+\text{Ar}(1) \xrightarrow{k_{MC}} \text{Ar}_2^++\text{Ar}(1),$$
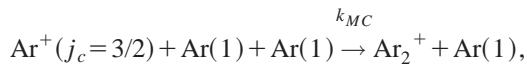
where Ar$^+$ has a core quantum number equal to $3/2$ because the only bounded level of Ar$_2^+$ produces Ar$^+(j_c=3/2)$ and Ar(1) by dissociation (Stephan *et al.* [54]) as shown by Fig. 2. In all experimental values of the reaction rate k_{MC}, T_A is of the order of 300 K. Johnsen *et al.* [55] have measured the latter at 80 K and 320 K according to the value of j_c demonstrating obviously the predominant reaction with Ar$^+(j_c=3/2)$. Assuming a temperature dependence of k_{MC} under the form (Moratz *et al.* [56]),
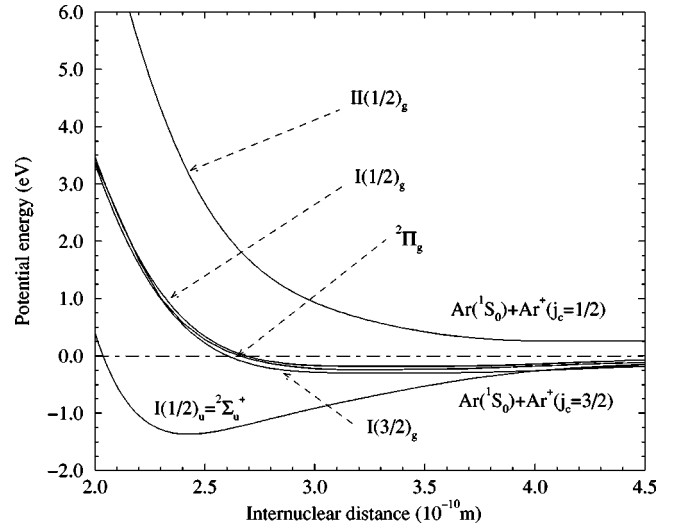
FIG. 2. Some potential energy curves of Ar$_2^+$ including the spin-orbit coupling effects.

$$k_{MC}(T_A)=k_0\left(\frac{T_A}{T_0}\right)^{-m}, \quad (13)$$

the results of Johnsen *et al.* yield to $k_0=2.9 \times 10^{-43}$ m^6 s^{-1}, $T_0=300$ K, and $m=0.41$. The exponent thus calculated is not correlated with the one of the reaction rate cited by Lam *et al.* [12] derived from the work of Shon *et al.* [57],

$$k_{MC}(T_A)=2.5\times 10^{-43}\left(\frac{T_A}{300}\right)^{-1.5} \text{ m}^6 \text{ s}^{-1}.$$

Since this rate coefficient has been calculated for temperatures higher than 300 K, this form was adopted.

An other important production process is the metastable-metastable associative ionization,

$$\text{Ar}(3p^54s)+\text{Ar}(3p^54s) \xrightarrow{k_{MAI}} \text{Ar}_2^++e^-.$$
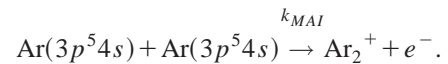
The value of the reaction rate is given by Neeser *et al.* [58] and Bogaerts and Gijbels [8] at the temperature of 300 K: $k_1=6.3\times 10^{-16}$ m^3 s^{-1}. This coefficient decreases when T_A increases. We have assumed a temperature dependence in the same way than Eq. (13) with $k_0=k_1$, $T_0=300$ K, and $m=0.5$ that is,

$$k_{AI}(T_A)=6.3\times 10^{-16}\left(\frac{T_A}{300}\right)^{-0.5} \text{ m}^3 \text{ s}^{-1}.$$

The associative ionization of Hornbeck-Molnar,

$$\text{Ar}(n_g \geqslant 20)+\text{Ar}(1) \xrightarrow{k_{HM}} \text{Ar}_2^++e^-, \quad (14)$$
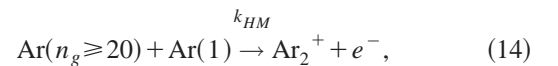
has to be discussed. All levels for which the energy is greater than the ionization potential to form Ar$_2^+$ ions can give rise to this process.

At $T_A = 300$ K, Becker and Lampe [59] have determined the mean rate coefficient,

$$k_{HM} = 2 \times 10^{-15} \quad \text{m}^3 \text{ s}^{-1}.$$

Its determination from this value for higher temperature is difficult due to the large number of levels involved and to the cross sections that present the particularity to strongly depend on the principal quantum number.

The case of alkali Rydberg atoms for the associative ionization has been extensively studied (Kumar *et al.* [60]). In a recent paper (Bultel and Vervisch [61]), we have developed a quasiclassical model based on the approach of Weiner and Boulmer [62] for Na_2^+ formation. This model assumes that the process (14) occurs for Rydberg levels when the kinetic energy of the incoming ground-state atom is sufficient to overcome the repulsive potential. This atom approaches of the core of $Ar(n_g)$ at a distance shorter than the classical radius of the orbit of the Rydberg electron. When the distance is suitable, the core and the atom bind. The exceeding energy is transferred to the outer electron by a virtual photon that leads the process to be similar to the photoionization. The electron leaves the Ar_2^+ molecular ion so formed. The results show that k_{HM} decreases deeply while T_A increases. Therefore, the Hornbeck-Molnar process is neglected here.

Ar_2^+ can be destroyed by dissociative recombination,

$$Ar_2^+ + e^- \xrightarrow{k_{DR}} Ar(1) + Ar(1), \tag{15}$$
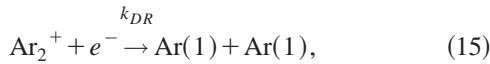
for which Mehr and Biondi [63] have determined the rate coefficient:

$$k_{DR}(T_e, T_A) = 8.5 \times 10^{-13} \left(\frac{T_e}{300} \right)^{-0.67} \left(\frac{T_A}{300} \right)^{-0.58} \quad \text{m}^3 \text{ s}^{-1},$$

k_{DR} depends on T_A because of the transient step of the reaction (15): $Ar^+ + Ar(1) + e^-$. We have also considered the following mechanism:

$$Ar_2^+ + e^- \xrightarrow{k_{DR}^*} Ar(i > 1) + Ar(1). \tag{16}$$
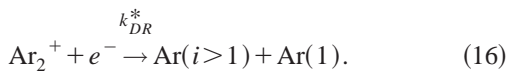
Its rate coefficient has been given by Ustinovskii and Kholin [64] at 300 K,

$$k_{DR}^*(T_e, 300 \text{ K}) = 9.1 \times 10^{-13} \left(\frac{T_e}{300} \right)^{-0.61} \quad \text{m}^3 \text{ s}^{-1},$$

for all excited i levels. k_{DR}^* is the result of the summation of the partial rate coefficients over all excited levels of final states according to the probability for the final argon atom to be in a particular i value. Collier *et al.* [65] have indicated that the dissociative recombination mainly provides the formation of $3p^5 4s$ states whereas the branching ratios for excited argon atoms formation are not well known. We have, therefore, taken into account this process for the balance of Ar_2^+ and considered only its influence for the evolution of $[Ar(2 \leq i \leq 4)]$.

The processes (15) and (16) are very similar. A transient step like $Ar^+ + Ar(1) + e^-$ surely takes place for the process (16). We have hence assumed that

$$k_{DR}^*(T_e, T_A) = 9.1 \times 10^{-13} \left(\frac{T_e}{300} \right)^{-0.61} \left(\frac{T_A}{300} \right)^{-0.58} \quad \text{m}^3 \text{s}^{-1}.$$

Finally, the loss of Ar_2^+ may be due to the direct electronic dissociation,

$$Ar_2^+ + e^- \xrightarrow{k_{DD}} Ar^+ + Ar(1) + e^-,$$
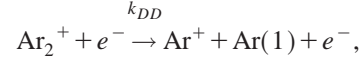
for which Marchenko [66] has calculated the cross section for weak temperature levels assuming equilibrium for the vibrational distribution of Ar_2^+.

Due to the selection transition rules and potential energy curves, two channels of dissociation are possible (see Fig. 2):

$$Ar_2^+[I(1/2)_u] + e^- \xrightarrow{k_{DD}(3/2)} Ar_2^+[I(1/2)_g] + e^-$$
$$\Rightarrow Ar^+(j_c = 3/2) + Ar(1) + e^-, \tag{17a}$$

$$Ar_2^+[I(1/2)_u] + e^- \xrightarrow{k_{DD}(1/2)} Ar_2^+[II(1/2)_g] + e^-$$
$$\Rightarrow Ar^+(j_c = 1/2) + Ar(1) + e^-, \tag{17b}$$
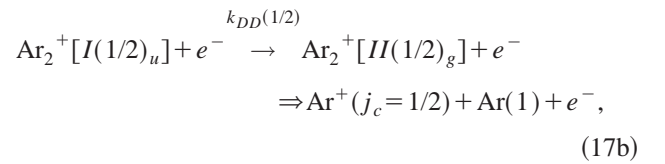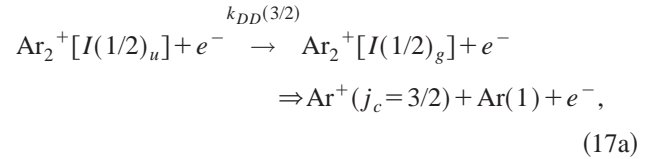
where the major contribution is provided by the process (17a) at low temperatures.

Ivanov [67] has experimentally studied the destruction of Ar_2^+ ions by electrons in a self-sustained gas discharge. He has determined the rate coefficient as a function of T_e. Its calculation from the cross section proposed by Marchenko gives results less than those experimentally determined. He explains this result as a nonequilibrium effect of the $Ar_2^+(v)$ distribution resulting of the competition between dissociative recombination and vibrational relaxation in Ar_2^+ collisions with the plasma particles. For temperatures higher than 11×10^3 K, he has pointed out the major role of the direct dissociation of molecular ions in relation to dissociative recombination.

The level of temperature of interest being less than 11×10^3 K, we have adopted the results of Marchenko rather than those of Ivanov and calculated the rate coefficient for the electronic temperature assuming equilibrium. We have moreover separated both channels (17a) and (17b), this latter requiring more energy due to the splitting of the core configurations. The mathematical form of the rate coefficients calculated in this way is

$$k_{DD}(j_c, T_e) = 1.36 \times 10^{-12}$$
$$\times \exp\left[-\frac{24\,300 + (\frac{3}{2} - j_c) \times 10^4}{T_e} \right] \quad \text{m}^3 \text{ s}^{-1}.$$

IV. RESULTS AND DISCUSSION

Assuming the electroneutrality, the previous mechanisms lead to calculate the time evolution of $[\mathrm{Ar}(i)]$ for $1 \le i \le 68$ according to the balance derived from Eq. (1) where the speed and $\vec{J}_i$ are assumed equal to 0. It necessitates the calculation of rate coefficients (Decoster *et al.* [68]). For excitation, the rate coefficient denoted C is derived from the cross section by

$$C^{e,A} = \sqrt{\frac{8 k_B T_{e,A}}{\pi \mu}} \int_{x_{min}}^{+\infty} x \, e^{-x} \sigma^{e,A}(x) \, dx,$$

where k_B is the Boltzmann constant, μ the reduced mass of the system of particles in interaction (m_e for a collision between an electron and an atom, $m_A/2$ for a collision between heavy particles), and $x = \epsilon/(k_B T_{e,A})$. The rate coefficient for radiative recombination [due to Eqs. (2) and (3)] and ionization by atoms or electrons are calculated by this way.

For inverse processes, the rate coefficient C' is derived from detailed balance,

$$(C^{e,A})' = C^{e,A} \frac{g_k}{g_l} \exp\left(\frac{E_{lk}}{k_B T_{e,A}}\right),$$

with $l > k$. For the recombination involving an electron as third particle, the rate coefficient is derived from the Saha equilibrium equation,

$$(C_{i\text{-ion}}^e)' = C_{i\text{-ion}}^e \frac{g_i}{g_e \, g_{\text{ion}}(j_c)} \left(\frac{h^2}{2 \pi m_e k_B T_e}\right)^{3/2}$$

$$\times \exp\left[\frac{E_{\text{ion}}(j_c) - E(i)}{k_B T_e}\right]. \qquad (18)$$

The case of three-body recombination with an atom is different. Collins [69] has verified in a plasma at high pressure with $T_e \neq T_A$ that the Saha equilibrium ionization equation is slightly modified as follows:

$$\frac{n_e n_{\text{ion}}}{n_i} = \frac{g_e \, g_{\text{ion}}}{g_i} \left(\frac{h^2}{2 \pi m_e k_B T_e}\right)^{-3/2} \exp\left[-\frac{E_{\text{ion}} - E(i)}{k_B T_A}\right].$$

This is due (Cleland and Meeks [70]) to the translation partition function of electrons in which T_e appears [term in $(h^2/2\pi m_e k_B T_e)^{-3/2}$] and to the excitation that only depends on T_A in the case of a strong predominance of heavy particles collisions. Therefore, the rate coefficient has been calculated from Eq. (18) replacing T_e by T_A in the exponential term.

Finally, the time evolution of $[\mathrm{Ar}(i)]$ is calculated with "LSODE" (Livermore solver for ordinary differential equation), which is a very convenient tool for this kind of transient problem (Bourdon and Vervisch [71]).

A. Plasma with high ionization degree

The case of plasmas with a high ionization degree may be a test of the global consistency of the model. Marie [9] has measured the population density of the excited levels over a
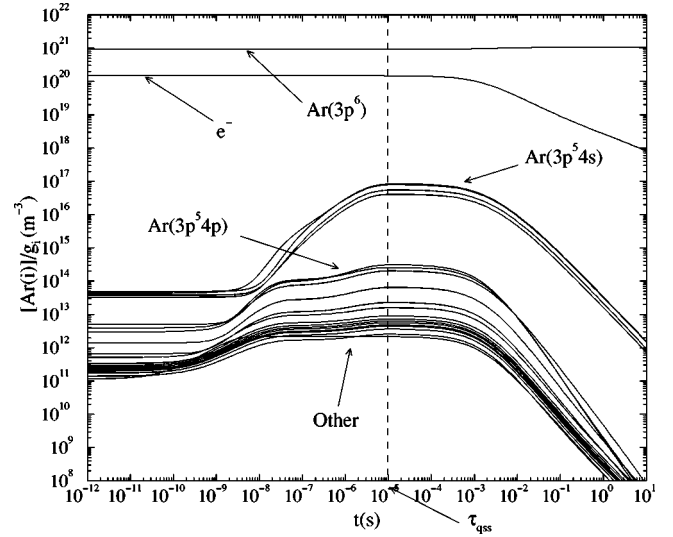
FIG. 3. Time evolution of densities divided by their statistical weight for Marie's conditions: $n_e = 1.5 \times 10^{20}$ m^{-3}, $T_e = 5500$ K, $T_A = 2000$ K, and $[\mathrm{Ar}(1)] = 9 \times 10^{20}$ m^{-3}. Note that the quasi-steady-state time τ_{qss} is 10^{-5} s. The electron density is shown directly instead of n_e/g_e as $[\mathrm{Ar}^+]$.

wide range of energy in a recombining argon plasma with $n_e = 1.5 \times 10^{20}$ m^{-3}, $[\mathrm{Ar}(1)] = 9 \times 10^{20}$ m^{-3}, $T_e = 5600$ K, and $T_A = 2000$ K. In such conditions, an equilibrium distribution is observed according to an excitation temperature equal to the electron one.

For the previous values of n_e, T_e, and $[\mathrm{Ar}(1)]$, Fig. 3 shows the temporal evolution for the various $[\mathrm{Ar}(i)]$ for a recombining situation: the atomic level population densities are assumed to be initially in equilibrium at the electron temperature but in concentrations lower than those calculated from Saha equation. All Ar$_2^+$ processes have been removed and the Drawin's equation (4) for the electron induced excitation for the allowed transitions has been used. These population densities exhibit a quasi-steady-state having a duration of 1 ms beyond $\tau_{qss} = 10^{-5}$ s. It is important to note that the initial conditions of the calculation has no influence on τ_{qss} and the duration of the quasi-steady-state. In this experiment, the hydrodynamic time of $[\mathrm{Ar}(i)]$ ($\tau_v \simeq 10^{-4}$ s) is greater than τ_{qss}. Therefore, the population densities measured by Marie have to be compared with those calculated by the CR model in the quasi-steady-state.

The Boltzmann graph of Fig. 4 illustrates this comparison when the quasi-steady-state is achieved. Except for some $3p^5 4p$ levels, the agreement is satisfactory. Almost all groups are in partial equilibrium according to the temperature T_e accounting for the major contribution of the electron induced processes for the excitation. We have noted that the model of Vriens and Smeets for the electron induced excitation between radiatively coupled levels gives no better accordance with the experimental distribution while the model of Seaton leads to large discrepancies with respect to the measurements of Marie. Finally, as a result of the high ionization degree, the role of the atom induced processes is negligible. In the following, we have used systematically the expressions proposed by Drawin for the allowed transitions. Con-
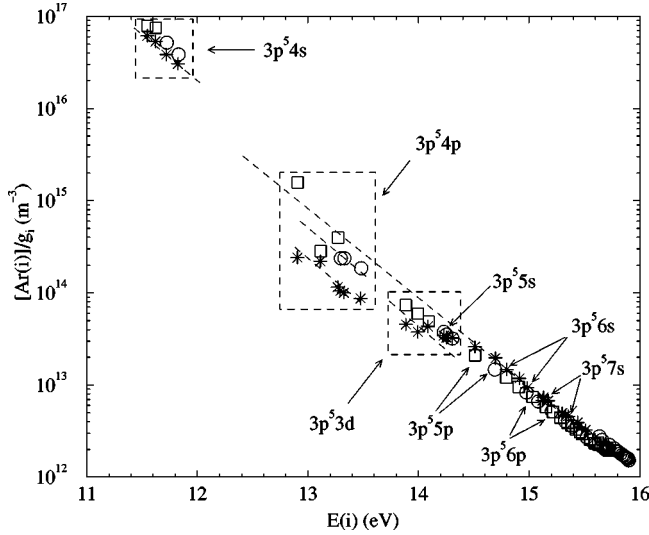
FIG. 4. Boltzmann plot calculated by the CR model using Drawin's equations for electron induced excitation for allowed transitions under the Marie conditions and experimental distribution (asterisks). Circles and squares denote, respectively, the states with $j_c = 1/2$ and $j_c = 3/2$. The dashed line illustrates partial equilibrium for the excitation temperature $T_{exc} = T_e$.

sidering the Ar_2^+ processes changes deeply the temporal evolution of the population densities up to 2×10^{-5} s as shown in Fig. 5. This result is obtained assuming that Ar_2^+ is initially in equilibrium with other ions corresponding to a slightly higher n_e to obtain the same electron density in quasi-steady-state. The evolution before 2×10^{-5} s depends on the initial value of $[Ar_2^+]$ as discussed in the following. The dissociative recombination (16) towards the metastable levels leads to an over concentration of all excited levels below this limit. Then, their population densities join the values obtained without Ar_2^+ processes. Afterwards, the time evolution remains the same one so that beyond τ_{qss}
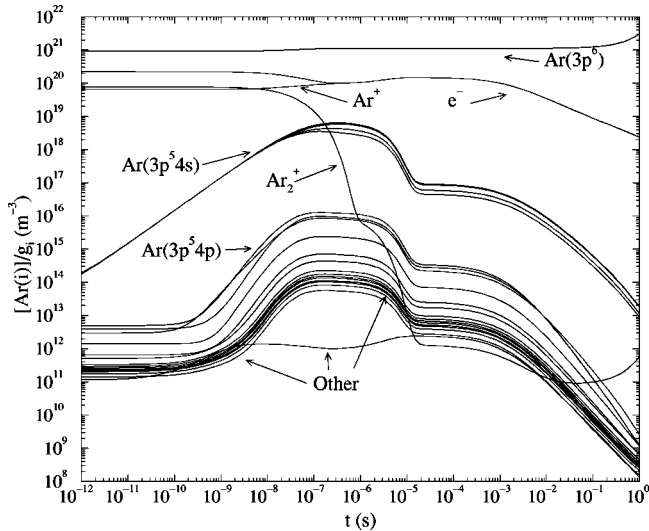
FIG. 5. Same as Fig. 3 considering all Ar_2^+ processes. At $t = 0$, Ar_2^+ is assumed to be in equilibrium with the other ions.
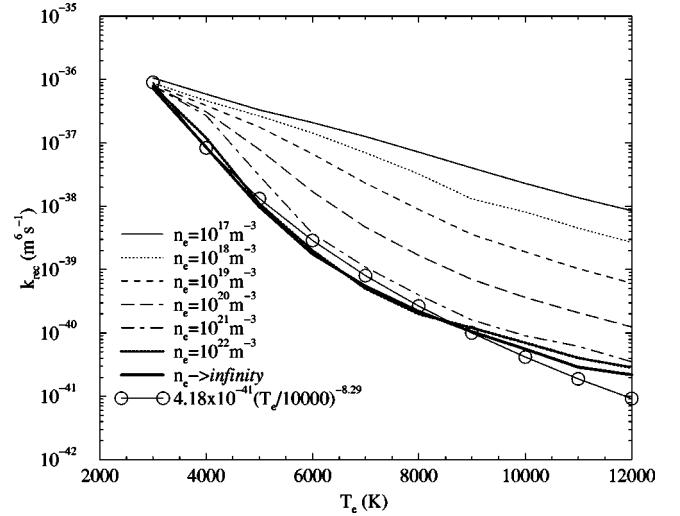
FIG. 6. Influence of the radiative processes on the calculation of the recombination rate coefficient.

$= 2 \times 10^{-5}$ s the quasi-steady-state occurs. For $t > 10^{-2}$ s, the temporal evolutions of the population densities become again different of those calculated neglecting the role of Ar_2^+. Finally, this molecule has no influence on the characteristics of the quasi-steady-state for highly ionized plasmas, which confirms the validity of our model.

B. The total recombination rate coefficient k_{rec}

The previous behavior allows the determination of the total recombination rate coefficient k_{rec}. When the electron density is sufficiently high the role of Ar_2^+ is, therefore, negligible and all elementary processes are coupling together to ensure the global reaction,

$$Ar^+ + e^- + e^- \xrightarrow{k_{rec}} Ar + e^-.$$
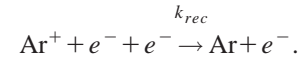
Removing all the Ar_2^+ processes in the model, this rate coefficient is defined as

$$k_{rec} = -\frac{1}{[Ar^+]n_e^2}\frac{d[Ar^+]}{dt} = -\frac{1}{n_e^3}\frac{dn_e}{dt}, \quad (19)$$

during the quasi-steady-state (Bourdon and Vervisch [71]). Meanwhile, we have checked that the depopulating rate $-d[Ar^+]/dt$ is also equal to the populating one $d[Ar(1)]/dt$. The degree of opacity of the plasma plays a significant role in depopulating processes. When τ_{qss} is achieved, the value of k_{rec} obtained from Eq. (19) depends not only on the electron temperature T_e but also on the density n_e. This behavior is illustrated by Fig. 6 showing the rate coefficient obtained for various (n_e, T_e). k_{rec} is all the smaller that n_e is greater. For $n_e = 10^{22}$ m^{-3}, the electron density is sufficiently high to lead a quasi-independence of the result on n_e. When the electron density tends to infinity, k_{rec} tends itself to the limit for which the radiative processes are completely negligible: k_{rec} depends on T_e only. The
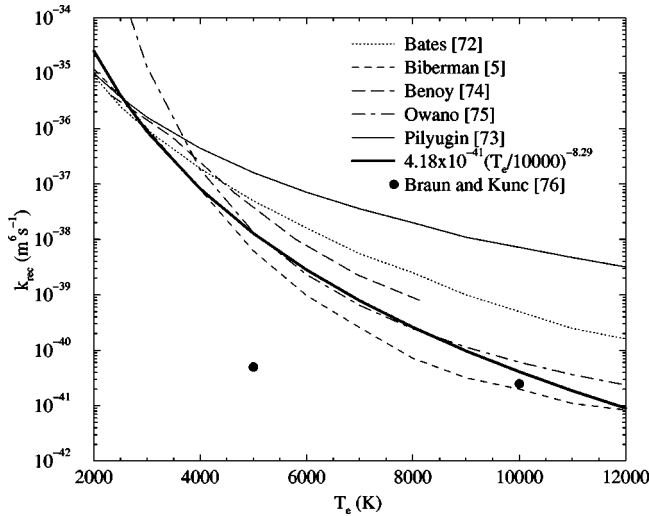
FIG. 7. Comparison between the T_e^{-x} fitted law determined from the present CR model and other reference data.

value adopted is thus this one and is confirmed by a direct remove of all radiative processes in the CR model.

For the implementation of k_{rec} in numerical codes of argon plasma flows, we have fitted the results with the simple law following T_e^{-x},

$$k_{rec} = 4.18 \times 10^{-41} \left(\frac{T_e}{10\,000} \right)^{-8.29} \text{m}^6 \text{s}^{-1}, \qquad (20)$$

for the electron temperature range 3000–12 000 K studied here. Figure 6 shows that the discrepancy with the results from the CR model does not exceed a factor of 2.

There exists a lot of experimental and theoretical data concerning the recombination rate coefficient. Figure 7 illustrates the comparison between our fitted law and several reference data. Bates *et al.* [72] have determined the recombination rate coefficient for pseudoalkali and for hydrogen ion plasmas that may be applicable to other species. Our fitted law is in relatively good agreement with their results for low temperature. This is the case for the works of Pilyugin and Pilyugin [73] that are based on atomic theory of gases considerations. But the discrepancy for higher temperature is significant. Results of Bates *et al.* are based upon a quasi-equilibrium steady-state approximation using the Gryzinski's cross sections for the inelastic processes assuming that these processes are classical and are as a result more related to ours than Pilyugin and Pilyugin.

Biberman *et al.* [5] have adopted a different approach. They have applied the theory of impact-radiation recombination (random walk of a recombining electron in the discrete space of the atom energy levels) in a low-temperature plasma. The result obtained for argon, shown in Fig. 7, is globally less than ours but in good accordance for low temperature.

Benoy *et al.* [74] have calculated k_{rec} following a hybrid procedure. Their main objective was to reduce the number of levels considered to simplify the calculation. A cutoff procedure is adopted in the energetic diagram for a level surely in

Saha equilibrium at the temperature T_e due to the electron induced ionization processes (5) whatever the conditions. The rate coefficient calculated in these conditions is plotted on Fig. 7 and agree well with those determined in the present paper for low T_e. For higher temperatures, they remain too high. The agreement is more satisfactory with the rate of Owano *et al.* [75] for electron temperature higher than 4000 K. These authors assume that the metastable $3p^5 4s$ states control the recombination process. This assumption, valid for high temperature, is done by Braun and Kunc [76]. From their three-level atomic model collisional-radiative calculation, they have determined the recombination coefficient for three electron temperatures 5000 K, 10^4 K, and 2.5 $\times 10^4$ K. Their result for $T_e = 10^4$ K is well correlated with our study as illustrated by Fig. 7. As a result of the number of excited levels considered, the k_{rec} value obtained for the lower electron temperature (5×10^{-41} m^6 s^{-1}) is far from the other reference data. For $T_e \geqslant 10^4$ K, a three-level model of recombining argon plasmas is, therefore, a satisfactory approximation. In conclusion, our fitting law is in good agreement with other works applicable to only a part of the range $2000 \leqslant T_e \leqslant 12\,000$ K studied here.

C. Weakly ionized plasma

van Ootegem [10] has recently studied a high-frequency-generated argon plasma jet expanded in a $p = 1700$ Pa vacuum chamber. He has measured n_e and T_e using Langmuir's probes and the population density of the excited levels by emission spectroscopy. For the maximum energy available by the power supply (high-energy condition in the following), the electron parameters are $T_e = 6000$ K ± 500 K and $n_e = (1.0 \pm 0.5) \times 10^{18}$ m^{-3} while $T_e = 5500$ K ± 500 K and $n_e = (3.0 \pm 2.0) \times 10^{17}$ m^{-3} were obtained in the case of a lower energy supplied by the torch (low-energy condition in the following). The heavy particles temperature
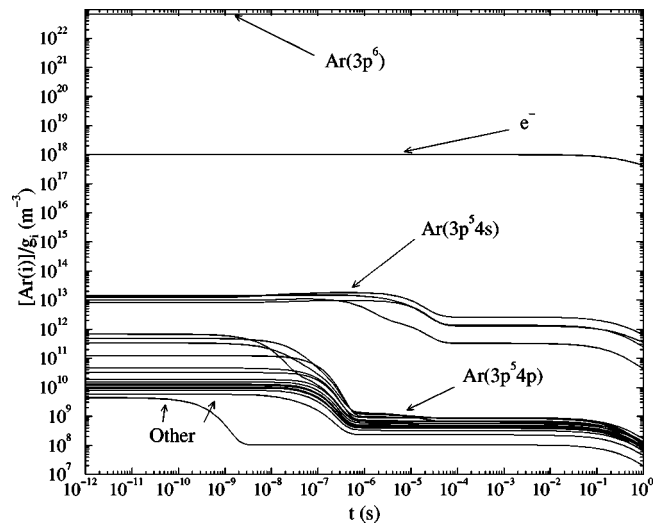
FIG. 8. Time evolution of densities for van Ootegem's conditions without considering Ar$_2^+$: $n_e = 10^{18}$ m^{-3}, $T_e = 6000$ K, $T_A = 1800$ K, and $[Ar(1)] = 6.8 \times 10^{22}$ m^{-3}. The quasi-steady-state is observed for $\tau_{qss} = 8 \times 10^{-5}$ s. The electron density is shown directly instead of n_e / g_e.
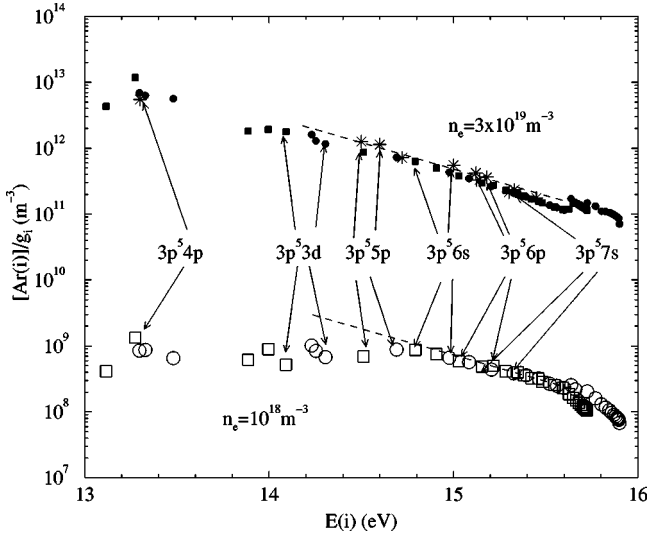
FIG. 9. Boltzmann plot calculated by the CR model using Drawin's equations under the van Ootegem's conditions with various n_e without considering the Ar_2^+ processes and experimental distribution (asterisks). Circles and squares denote, respectively, the states with $j_c = 1/2$ and $j_c = 3/2$ for the experimental electron density $n_e = 3 \times 10^{17}$ m^{-3} (nonfilled symbols) and for a hypothetical electron density $n_e = 3 \times 10^{19}$ m^{-3} (filled symbols). The dashed line illustrates partial equilibrium for the excitation temperature $T_{exc} = T_e$.

is estimated to be $T_A = 1800$ K for both conditions and the excited level concentrations $[Ar(i)]$ exhibit an equilibrium distribution with $T_{exc} \simeq T_e$.

Figure 8 shows the temporal evolution obtained for the high-energy condition without considering the Ar_2^+ processes. The calculation starts from an equilibrium without importance for the distribution observed in quasi-steady-state. Note that τ_{qss} is equal to 8×10^{-5}s for the $3p^54s$ levels including the metastable ones while $\tau_{qss} = 8 \times 10^{-7}$s for the more excited. Figure 9 illustrates the comparison be-
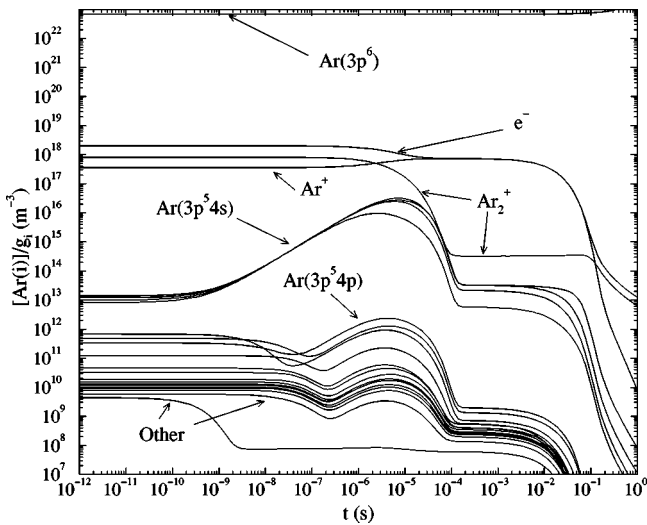
FIG. 10. Same as Fig. 8 considering all Ar_2^+ processes. The quasi-steady-state is observed for $\tau_{qss} = 2 \times 10^{-4}$ s.
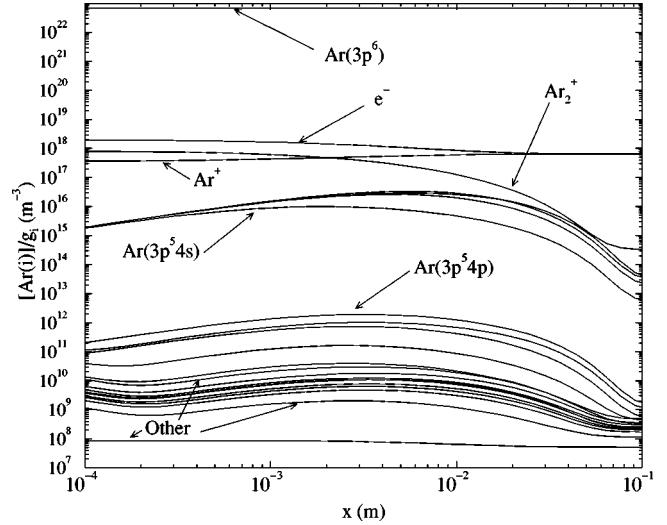
FIG. 11. Axial distribution obtained from the time evolution shown in Fig. 10 and from Eq. (21).

tween the $[Ar(i)]$ distributions in quasi-steady-state. An equilibrium with $T_{exc} = T_e$ is obvious for levels having an excitation energy higher than 15 eV but the order of magnitude of density is too low of a factor of 10^3 for the more excited. Conversely, if we try to determine the electron density leading to the experimental distribution, the best agreement is obtained with $n_e = 3 \times 10^{19}$ m^{-3} and $T_e = 5500$ K as shown by Fig. 9.

When the processes involving Ar_2^+ are taken into account, the analysis is more complicated than the previous
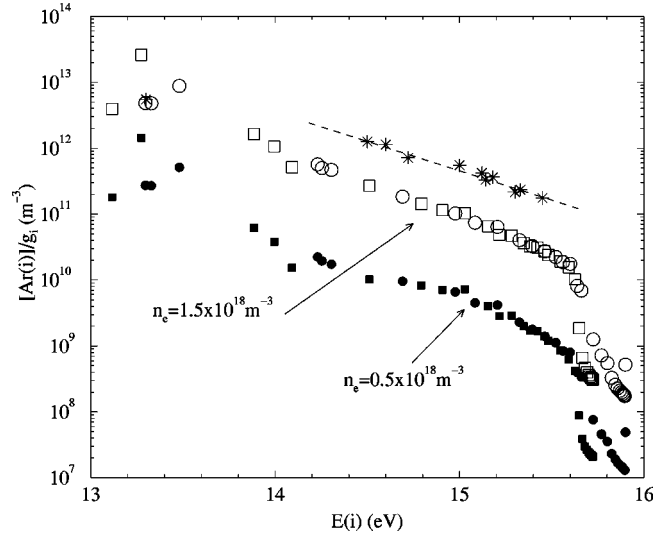
FIG. 12. Distributions calculated by the CR model using Drawin's equations under van Ootegem's high-energy condition considering the Ar_2^+ processes when $[Ar(3p^54s)]$ is maximum and experimental distribution (asterisks). The electron density varies along its uncertainty's range showing the sensitivity of the calculation: the nonfilled symbols denote the results obtained with $n_e = 1.5 \times 10^{18}$ m^{-3} and the filled ones denote those obtained with $n_e = 0.5 \times 10^{18}$ m^{-3}. Circles and squares denote, respectively, the states with $j_c = 1/2$ and $j_c = 3/2$.

one. The time evolution of the different densities depends on the initial condition for $[Ar_2{}^+]$. Below 10^{15} m^{-3} for both conditions of van Ootegem, Ar$_2{}^+$ has no influence, the temporal evolution is the same as Fig. 8. For $[Ar_2{}^+]_{t=0} = 10^{16}$ m^{-3}, an increase of concentrations followed by a decrease is observed for $t = \tau_m \simeq 10^{-5}$ s. The quasi-steady-state occurs when $t = \tau_{qss} \simeq 10^{-4}$ s. The moment at which the previous extremum of densities is observed depends slightly on $[Ar_2{}^+]_{t=0}$ but the higher the $[Ar_2{}^+]_{t=0}$ the smaller the moment. At the same time, these extremum of $[Ar(i)]$ are all the greater. Whatever its order of magnitude, this initial concentration of Ar$_2{}^+$ has no influence on τ_{qss}. Figure 10 shows the time evolution of the various excited level population densities calculated by the CR model for the high-energy condition when the electron density is $n_e = 10^{18}$ m^{-3} near τ_m, Ar$_2{}^+$ being assumed initially in equilibrium with other ions. This level of $[Ar_2{}^+]_{t=0}$ is the greater one compatible with the assumptions adopted in our model. With respect to Fig. 8, the quasi-steady-state begins later for the excited levels: the population densities present a decrease after $\tau_m = 4 \times 10^{-6}$s. This behavior is due again mainly to the dissociative recombination that overpopulates the metastable states leading to an important increase of higher excited level population densities under electron impact. Moreover, we can note that the temporal evolutions for $t \geq \tau_{qss}$ are different than those in Fig. 8 where Ar$_2{}^+$ is not considered. It is important to note that this discrepancy was not observed in the experimental condition of Marie where the electron density is higher. This is due to the fact that $[Ar_2{}^+]$ is much greater in the present case for $t \geq \tau_{qss}$.

The hydrodynamic time scale τ_v is shorter than for Marie's experiment. Its determination has to be done accurately in order to compare the distributions calculated and those measured. A Navier-Stokes calculation of the jet, considered behaving like a hot gas without specific plasma characteristics as a result of the weakness of the ionization degree, shows that the speed v is close to 750 m s^{-1} at the location of measurements. Moreover, the velocity decreases in the downstream according to the linear law

$$v(x) = v_0 \left(1 - \frac{x}{X} \right), \qquad (21)$$

with $v_0 = 750$ m s^{-1} and $X = 0.35$ m. At time t, the fluid particle is thus at the location x such that

$$x = X(1 - e^{-v_0 t/X}).$$

Chang and Ramshaw [77] have numerically simulated non-equilibrium effects in an atmospheric argon plasma jet using the CR model of Braun and Kunc. They have pointed out that the higher the time scale for species density changes due to diffusion of Ar(i) (defined as $\tau_d = [Ar(i)] |\vec{\nabla} \cdot \vec{J}_i|^{-1}$) the smaller the population density of excited species. For the plasma of Chang and Ramshaw, the ionization degree is high due to the pressure level and the heating power. τ_d varies as a result over the range $10^{-4} - 10^{-3}$ s. In our conditions, τ_d is much more important: the diffusion is therefore inopera-

tive for varying the population densities in balance equation (1). Moreover, the previous fit for the velocity indicates that the time scale due to fluid expansion or contraction $\tau_e = |\vec{\nabla} \cdot \vec{v}|^{-1}$ is of the same order of magnitude. The related term in Eq. (1) also being negligible, the axial population density distribution $[Ar(i)]$ is derived directly from the temporal evolution of Fig. 10 where time t is replaced by x location neglecting the influence of v on $[Ar(1)]$ due to the mass balance equation (see Fig. 11). The axial resolution of the spectroscopic device is $\Delta x = 10^{-3}$ m. For this length, the populations are the same as those calculated in Fig. 10 near 3×10^{-6} s. We deduce that the mechanical time scale is such that $10^{-6} < \tau_v < 10^{-5}$ s and that the population densities of interest are those calculated in the vicinity of τ_m instead of τ_{qss}.

The distribution thus considered is very sensitive to the electron density. For the range of n_e provided by the experimental uncertainty, Fig. 12 illustrates for $t = \tau_m$ the different distributions related to the model that vary over an order of magnitude. As for the Marie's conditions, the atom inelastic processes are negligible. In the case of the low-energy condition, Fig. 13 shows obvious discrepancies between the calculated and experimental distributions in spite of considering the uncertainty range. We can note that inelastic atom processes begin to play a significant role as shown by the distribution at high energy. Nevertheless, the low discrepancy observed under the high-energy condition is relatively satisfactory considering the high sensibility of the model's result towards n_e.

The concentrations of the various Ar(i) depends on $[Ar_2{}^+]_{t=0}$. We obtain the best agreement between calculated distributions at $t = \tau_m$ and experimental distributions assuming that Ar$_2{}^+$ is initially in equilibrium with other ions. Since the important process is the dissociative recombination leading to a global loss of Ar$_2{}^+$ over the time scales considered here, $[Ar_2{}^+]_{t=0}$ adopted has to be justified. The densities
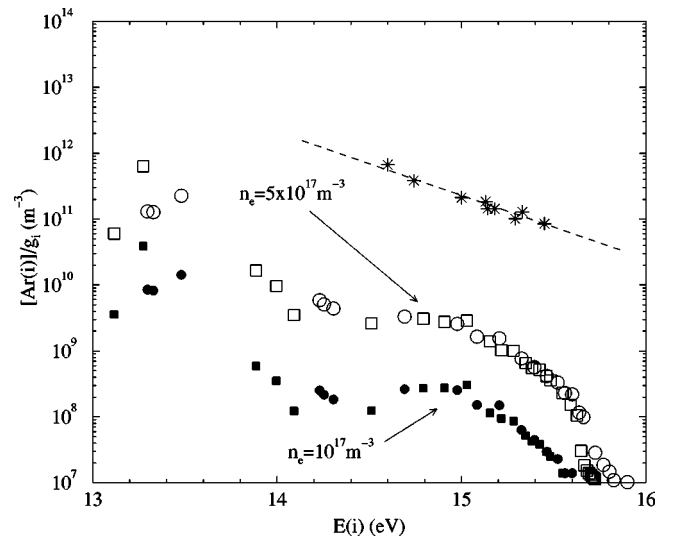
FIG. 13. Comparison between calculated and experimental distributions under the low-energy condition of van Ootegem. The symbols are the same as in Fig. 12.
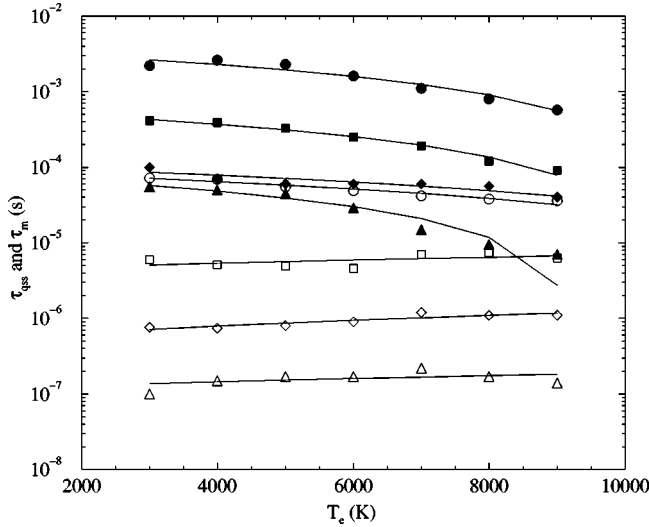
FIG. 14. Quasi-steady-state time τ_{qss} (filled symbols) and time for maximum population densities τ_m (open symbols) versus electron temperature for various values of n_e. The population density of the ground state is the same as in the van Ootegem's high-energy conditions. The symbols circles, squares, diamonds, and triangles denote, respectively, the conditions $n_e = 4 \times 10^{16}$ m^{-3}, 4×10^{17} m^{-3}, 4×10^{18} m^{-3}, and 4×10^{19} m^{-3}. Each line illustrates a linear regression showing the mean behavior.

measured are of course highly dependent on the processes occuring in the torch where the plasma is created. The ionization conditions involved exceed largely the scope of the CR model developed in this paper. Indeed the pressure level in this region ($p = 15$ kPa) as well as the high-frequency electromagnetic source lead to disagreement with two fundamental assumptions: the kinetic scheme (Ustinovskii and Kholin [64]) and the maxwellian equilibrium distribution for electrons (Loffhagen *et al.* [78]). These aspects will be the subject of a future study.

D. Comments on τ_{qss} and τ_m

The previous case of low-energy condition has pointed out the importance of the hydrodynamic time with respect to the quasi-steady-state one in the comparison between numerical and experimental results. We have shown the importance of the electron density on τ_{qss} before. Figure 14 illustrates further the dependence of τ_{qss} on T_e with n_e as a parameter when Ar$_2^+$ is initially in equilibrium with other ions. This characteristic time is much more governed by the electron density than temperature. For $T_e \simeq 6000$ K, τ_{qss} is well given by the equation

$$\tau_{qss} = 10^{-5} \left(\frac{n_e}{10^{20}} \right)^{-0.61} \text{s}$$

over the range of electron density considered here ($10^{16} \leqslant n_e \leqslant 10^{20}$ m^{-3}).

In the same way, we can deduce an identical behavior for τ_m the time at which the maximum of the population densities are observed due to the influence of Ar$_2^+$ after they
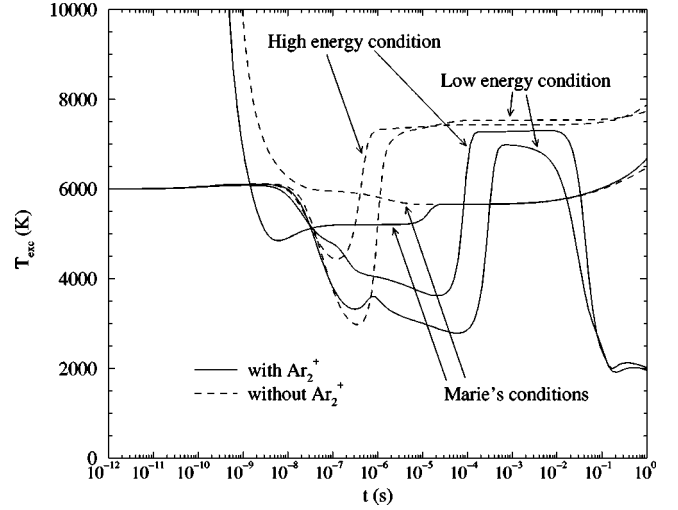
FIG. 15. Temporal evolution of the excitation temperature T_{exc} of the distribution of the excited level population densities in various conditions.

leave their initial value (see Fig. 14). In a general manner, the ratio τ_{qss}/τ_m is about 100 in order of magnitude. For very weakly ionized plasmas, the chemistry may be time-dependent even for short mechanical time scale.

E. Excitation temperature

It is interesting to discuss the characteristic temperature of the distribution of [Ar(i)] under the influence of Ar$_2^+$. The excitation temperature is defined as the parameter T_{exc} in the equilibrium Boltzmann law,

$$\frac{[\text{Ar}(j)]}{[\text{Ar}(i)]} = \frac{g_j}{g_i} \exp\left(-\frac{E_{ji}}{k_B T_{exc}} \right).$$

Figure 15 presents the time evolutions of T_{exc} with and without considering the influence of Ar$_2^+$. The energy range for which T_{exc} has been calculated is $14.75 - 15.5$ eV. The influence of Ar$_2^+$ is obvious for time t between 5×10^{-7} and 5×10^{-5} s in order of magnitude: the temperature T_{exc} is close to 4000 K for high-energy condition instead of 7300 K when the molecular ion is not taken into account whereas $T_{exc} \simeq 3000$ K for low-energy condition. Systematically, the excitation temperatures obtained before τ_{qss} considering Ar$_2^+$ are less than those without the relevant processes. This is the result of the excitation by electron impact from the metastable levels further populated by dissociative recombination towards levels close to them. The electron density being higher, this effect occurs in a similar but reduced way in the case of the Marie's conditions as shown in Fig. 15. When n_e is sufficiently high, the low difference between excitation temperature before and after τ_{qss} indicates that an excitation equilibrium is achieved more rapidly than the quasi-steady-state. Conversely to the case of the weakly ionized plasma, Ar$_2^+$ has absolutely no influence on T_{exc} during the quasi-steady-state. Therefore, to liken T_e and T_{exc} is obviously questionable.

V. CONCLUSIONS

In this paper, we have studied thoroughly the influence of the molecular ion Ar$_2$$^+$ on chemical behavior of a low-pressure recombining argon plasma jet in various conditions. This examination has been done using a collisional-radiative model where electron induced processes have been updated carefully as well as those due to heavy particles inelastic collisions. For a particular experimental situation, we have shown that the equilibrium and the order of magnitude observed for the highly excited level population densities may be understood involving the reactions provided by Ar$_2$$^+$ even if more information is needed to explain initially a sufficient level of its density. The dissociative recombination of Ar$_2$$^+$ appears to be an efficient process to overpopulate metastable states leading to the increase of more highly excited level number densities by electron impact.

For high electron density, our study has allowed a determination of the three-body recombination rate coefficient proposed under an analytical form for calculation purposes in satisfactory agreement with other data over a wide range of conditions. We have put forward the importance of the quasi-steady-state time τ_{qss} and its relation with the other time scale of the flow. Moreover, we have shown that τ_{qss}

has not to be achieved for comparison with experiments when the velocity of the flow is high and the ionization degree low. This behavior has to be considered when T_e is derived from excitation temperature.

Nevertheless, the discrepancies between calculated and experimental population number densities particularly in low n_e condition indicate that improvements are needed, we think mainly to the dissociative recombination rate coefficient. Today, the branching ratios allowing the accurate determination of the products are not well known. In this paper, we have assumed that only the recombination towards the $3p^54s$ states involving the metastable ones occur. If the potential curves of excited Ar$_2$ are suitable, the formation of more excited argon atoms, on $3p^54p$, $3p^53d$, or $3p^55s$ states for instance as experimentally pointed out by Guna *et al.* [79], Hardy [80], and Ramos *et al.* [81], is possible: it may lead to a direct overpopulation of the related number densities and consequently to a better agreement with experimental data. On the other hand, an experimental determination of [Ar$_2$$^+$] by induced laser photodissociation (Stevens *et al.* [82] and Moseley *et al.* [83]) is expected in the future to test the order of magnitude calculated by the CR model as well as the one needed as initial condition.

[1] M. Litvak and D. Edwards, J. Appl. Phys. **37**, 4462 (1966).

[2] J. Sarrette, A. Gomes, and J. Bacri, J. Quant. Spectrosc. Radiat. Transf. **53**, 143 (1995).

[3] F. Debal, J. Bretagne, M. Jumet, M. Wautelet, J. Dauchot, and M. Hecq, Plasma Sources Sci. Technol. **7**, 219 (1998).

[4] J. Kunc and W. Soon, Phys. Rev. A **40**, 5822 (1989).

[5] L. Biberman, V. Vorob'ev, and I. Yakubov, Sov. Phys. Usp. **15**, 375 (1973).

[6] H. Drawin, Z. Phys. **225**, 470 (1969).

[7] A. Bogaerts and R. Gijbels, Phys. Rev. A **52**, 3743 (1995).

[8] A. Bogaerts and R. Gijbels, J. Appl. Phys. **86**, 4124 (1999).

[9] J.-J. Marie, Ph.D. thesis, Université de Rouen, 1983.

[10] B. van Ootegem, Ph.D. thesis, University of Rouen, 2001.

[11] D. Freeman and K. Yoshino, J. Chem. Phys. **71**, 1780 (1979).

[12] S. Lam, C. Zheng, D. Lo, A. Dem'yanov, and A. Napartovich, J. Phys. D **33**, 242 (2000).

[13] H. Brunet, B. Lacour, J.R. Serra, M. Legentil, S. Mizzi, S. Pasquiers, and V. Puech, J. Appl. Phys. **68**, 4474 (1990).

[14] J. Yates, W. Ermler, N. Winter, P. Christiansen, Y. Lee, and K. Pitzer, J. Chem. Phys. **79**, 6145 (1983).

[15] M. Castex, M. Morlais, F. Spiegelmann, and J. Malrieu, J. Chem. Phys. **75**, 5006 (1981).

[16] J. Vlček, J. Phys. D **22**, 623 (1989).

[17] A. Bogaerts, R. Gijbels, and J. Vlček, J. Appl. Phys. **84**, 121 (1998).

[18] K. Katsonis and H. Drawin, report, 1976.

[19] W. Wadt, J. Chem. Phys. **68**, 402 (1978).

[20] W. Wiese, M. Smith, and B. Miles, *Atomic Transition Probabilities*, NSRDS Natl. Bur. Stand. (U.S.) Circ. No. 22 (U.S. GPO, Washington, DC, 1969), Vol. II.

[21] W. Wiese, J. Brault, K. Danzmann, V. Helbig, and M. Kock, Phys. Rev. A **39**, 2461 (1989).

[22] D. Verner, E. Verner, and G. Ferland, At. Data Nucl. Data Tables **64**, 1 (1996).

[23] T. Bornath, M. Schlanges, F. Morales, and R. Prenzel, J. Quant. Spectrosc. Radiat. Transf. **58**, 501 (1997).

[24] D. Salzmann, *Atomic Physics in Hot Plasmas*, International Series of Monographs on Physics (Oxford University Press, Oxford, 1998).

[25] A. Kimura, H. Kobayashi, M. Nishida, and P. Valentin, J. Quant. Spectrosc. Radiat. Transf. **34**, 189 (1985).

[26] L. Vriens and A. Smeets, Phys. Rev. **22**, 940 (1980).

[27] M. Seaton, *Atomic and Molecular Processes* (Academic Press, New York, 1962), p. 374.

[28] H. Straub, P. Renault, B. Lindsay, K. Smith, and R. Stebbings, Phys. Rev. A **52**, 1115 (1995).

[29] R. Schappe, M. Schulmann, L. Anderson, and C. Lin, Phys. Rev. A **50**, 444 (1994).

[30] D. Filipovic, B. Marinkovic, and L. Vuskovic, J. Phys. B **33**, 2081 (2000).

[31] A. Chutjian and D. Cartwright, Phys. Rev. A **23**, 2178 (1981).

[32] K. Tachibana, Phys. Rev. A **34**, 1007 (1986).

[33] D. Madison, C. Maloney, and J. Wang, J. Phys. B **31**, 873 (1998).

[34] K. Bartschat and V. Zeman, Phys. Rev. A **59**, R2552 (1999).

[35] C. Maloney, J. Peacher, K. Bartschat, and D. Madison, Phys. Rev. A **61**, 022701 (2000).

[36] J. Boffard, G. Piech, M. Gehrke, L. Anderson, and C. Lin, Phys. Rev. A **59**, 2749 (1999).

[37] G. Piech, J. Boffard, M. Gehrke, L. Anderson, and C. Lin, Phys. Rev. Lett. **81**, 309 (1998).

[38] D. Filipovic, B. Marinkovic, V. Pejcev, and L. Vuskovic, J. Phys. B **33**, 677 (2000).

[39] I. Bogdanova and S. Yurgenson, Opt. Spektrosk. **68**, 730 (1990).

[40] A. Mityureva, N. Penkin, and V. Smirnov, Opt. Spektrosk. **66**, 463 (1989).

[41] J. Chilton and C. Lin, Phys. Rev. A **60**, 3712 (1999).

[42] H. Hyman, Phys. Rev. A **18**, 441 (1978).

[43] E. Montenegro, W. Melo, W. Meyerhof, and A. de Pinho, Phys. Rev. Lett. **69**, 3033 (1992).

[44] P. Haugsjaa and R. Amme, J. Chem. Phys. **52**, 4874 (1970).

[45] J. Thomson, Philos. Mag. **23**, 449 (1912).

[46] H. Drawin, Z. Phys. **211**, 404 (1968).

[47] H. Drawin, Z. Phys. **225**, 483 (1969).

[48] H. Drawin and F. Emard, Phys. Lett. **43A**, 333 (1973).

[49] V. Lebedev, J. Phys. B **31**, 1579 (1998).

[50] B. Kaulakys, J. Phys. B **24**, L127 (1991).

[51] B. Kaulakys, J. Phys. B **18**, L167 (1985).

[52] M. Weyhreter, B. Barzick, A. Mann, and F. Linder, Z. Phys. D: At., Mol. Clusters **7**, 333 (1988).

[53] V. Lebedev and I. Fabrikant, Phys. Rev. A **54**, 2888 (1996).

[54] K. Stephan, A. Stamatovic, and T. Mark, Phys. Rev. A **28**, 3105 (1983).

[55] R. Johnsen, A. Chen, and A. Biondi, J. Chem. Phys. **73**, 1717 (1980).

[56] T. Moratz, T. Saunders, and M. Kushner, Appl. Phys. Lett. **54**, 102 (1989).

[57] J. Shon, M. Kushner, G. Hebner, and G. Hays, J. Appl. Phys. **73**, 2686 (1993).

[58] S. Neeser, T. Kunz, and H. Langhoff, J. Phys. D **30**, 1489 (1997).

[59] P. Becker and F. Lampe, J. Chem. Phys. **42**, 3857 (1965).

[60] A. Kumar, B. Saha, C. Weatherford, and S.K. Verma, J. Mol. Struct.: THEOCHEM **487**, 1 (1999).

[61] A. Bultel and P. Vervisch, J. Phys. B **35**, 111 (2002).

[62] J. Weiner and J. Boulmer, J. Phys. B **19**, 599 (1986).

[63] F. Mehr and M. Biondi, Phys. Rev. **176**, 322 (1968).

[64] N. Ustinovskii and I. Kholin, Sov. Phys. Tech. Phys. **35**, 808 (1990).

[65] F. Collier, J. Leblond, F. Hoffbeck, and P. Cottin, J. Chem. Phys. **74**, 4372 (1981).

[66] V. Marchenko, Sov. Phys. JETP **58**, 292 (1983).

[67] V. Ivanov, Opt. Spectrosc. **73**, 374 (1992).

[68] A. Decoster, P. Markowich, and B. Perthame, *Modeling of Collisions*, Applied Mathematics (Gauthier-Villars, Paris, 1998).

[69] C. Collins, Phys. Rev. **158**, 94 (1967).

[70] T. Cleland and F. Meeks, Spectrochim. Acta, Part B **51**, 1487 (1996).

[71] A. Bourdon and P. Vervisch, Phys. Rev. E **54**, 1888 (1996).

[72] D. Bates, A. Kingston, and R. McWhirter, Proc. R. Soc. London, Ser. A **267**, 297 (1962).

[73] N. Pilyugin and A. Pilyugin, High Temp. **35**, 1 (1997).

[74] D. Benoy, J. van der Mullen, M. van de Sanden, B. van der Sijde, and D. Schram, J. Quant. Spectrosc. Radiat. Transf. **49**, 129 (1993).

[75] T. Owano and C. Kruger, AIAA J. **31**, 75 (1993).

[76] C. Braun and J. Kunc, Phys. Fluids **30**, 499 (1987).

[77] C. Chang and J. Ramshaw, Phys. Plasmas **1**, 3698 (1994).

[78] D. Loffhagen, G. Braglia, and R. Winkler, Contrib. Plasma Phys. **38**, 527 (1998).

[79] M. Guna, L. Simons, K. Hardy, and J. Peterson, Phys. Rev. A **60**, 306 (1999).

[80] K. Hardy, Phys. Rev. A **58**, 1256 (1998).

[81] G. Ramos, M. Schlamkowitz, J. Sheldon, K. Hardy, and J.R. Peterson, Phys. Rev. A **52**, 4556 (1995).

[82] W. Stevens, M. Gardner, A. Karo, and P. Julienne, J. Chem. Phys. **67**, 2860 (1977).

[83] J. Moseley, R. Saxon, B. Huber, P. Cosby, R. Abouaf, and M. Tadjeddine, J. Chem. Phys. **67**, 1659 (1977).